TrpML-mediated astrocyte microdomain Ca^{2+} transients regulate astrocyte-tracheal interactions in CNS

Zhiguo Ma and Marc R. Freeman*

Vollum Institute, Oregon Health and Science University, Portland, OR

* correspondence to: freemmar@ohsu.edu

Running title: Astrocyte Ca^{2+} signaling regulates trachea

Abstract

Astrocytes exhibit spatially-restricted near membrane microdomain Ca^{2+} transients in their fine processes. How these transients are generated, and how they regulate brain function *in vivo* remain unclear. Here we show that *Drosophila* astrocytes exhibit spontaneous, activity-independent microdomain Ca^{2+} transients in their fine processes. Astrocyte microdomain Ca^{2+} transients are mediated by the TRP channel TrpML, stimulated by reactive oxygen species (ROS), and can be enhanced in frequency by tyramine via the TyrRII receptor. Interestingly, astrocyte microdomain Ca^{2+} transients are closely associated with tracheal elements, which dynamically extend filopodia throughout the nervous system, and astrocyte microdomain Ca^{2+} transients precede retraction of tracheal filopodia. Loss of TrpML leads to increased tracheal filopodial numbers and growth, and increased ROS in the CNS. Basal levels of astrocyte microdomain Ca^{2+} transient signaling were regulated by the hypoxia-sensitive factor Sima/Hif-1α, providing a link between astrocyte-tracheal interactions and the molecular control of CNS gas exchange. We propose that local ROS production regulates tracheal dynamics through TrpML-dependent modulation of astrocyte microdomain Ca^{2+} transients, and in turn CNS gas exchange.

Introduction

Astrocytes exhibit two major types of Ca^{2+} signaling events, whole cell fluctuations and near membrane microdomain Ca^{2+} transients (Khakh and McCarthy, 2015). Whole-cell transients are coordinated across astrocyte networks and regulated by adrenergic receptor signaling (Ding et al., 2013; Ma et al., 2016; Paukert et al., 2014). Emerging data suggests these transients are important for state-dependent changes (Ding et al., 2013; Ma et al., 2016; Paukert et al., 2014; Srinivasan et al., 2015), and involve TRPA1 channels that regulate the insertion of neurotransmitter transporters like GAT-3 into the membrane to alter neurophysiology (Shigetomi et al., 2012). Whole-cell astrocyte Ca^{2+} transients in the *Drosophila* larval nervous system are also stimulated by the invertebrate equivalents of adrenergic transmitters, octopamine and tyramine. Octopamine and tyramine stimulate cell-wide astrocyte Ca^{2+} increase through the dual-specificity Octopamine-Tyramine Receptor (Oct-TyrR) and the TRP channel Water witch (Wtrw). This astrocyte-mediated signaling event downstream of octopamine and tyramine is critical for neuromodulation: astrocyte-specific elimination of Oct-TyrR or Wtrw blocks the ability of octopamine and tyramine to silence downstream dopaminergic neurons, and alters both simple chemosensory behavior and a touch-induced startle response (Ma et al., 2016). Adrenergic regulation of whole-cell astrocyte Ca^{2+} transients therefore appears to be an ancient and broadly conserved feature of astrocytes.

The mechanisms that generate astrocyte microdomain Ca^{2+} transients are not understood, nor are the precise *in vivo* roles for this type of astrocyte signaling event (Bazargani and Attwell, 2016; Khakh and McCarthy, 2015). In mammals, astrocyte microdomain Ca^{2+} transients occur spontaneously, do not require neuronal activity (Nett et al., 2002), depend on extracellular Ca^{2+} (Rungta et al., 2016; Srinivasan et al., 2015), and persist in cultured astrocytes, which has been used to argue they are cell-autonomous (Khakh and McCarthy, 2015; Nett et al., 2002). A careful analysis of IP_3R2 knockout mice revealed that while whole-cell astrocyte Ca^{2+} transients are altered in IP_3R2 nulls, astrocyte microdomain Ca^{2+} transients were largely normal, indicating that these astrocyte Ca^{2+} signaling events are genetically separable (Srinivasan et al., 2015).

A recent study described a close association of astrocyte microdomain Ca^{2+} transients with mitochondria, their suppression by pharmacological blockade of opening of the mitochondrial permeability transition pore (mPTP), and an enhancement of these transients by reactive oxygen species (ROS). These observations led to the proposal that astrocyte microdomain Ca^{2+} transients were generated by transient opening of the mPTP during oxidative phosphorylation, perhaps as a means to balance mitochondrial function with local metabolic needs (Agarwal et al., 2017).

In this study we report that *Drosophila* astrocytes exhibit spontaneous, activity-independent microdomain Ca^{2+} transients. We show they are enhanced by tyramine through the TyrRII tyramine receptor and mediated by the TRP channel TrpML. Astrocyte microdomain Ca^{2+} transients are associated with filopodia extending from CNS trachea, an interconnected set of tubules that allow for gas exchange, with Ca^{2+} transients being activated by ROS and facilitating filopodial retraction. Surprisingly, the transcription factor Sima/Hif-1α, which modulates tracheal growth under hypoxic conditions, is also required for astrocyte microdomain Ca^{2+} transients. This observation provides a mechanistic link between astrocyte Ca^{2+} signaling and key hypoxia signaling factors. We propose that local hyperoxia results in increased production of ROS, which in turn gates TrpML activity and facilitates tracheal retraction, thereby dynamically regulating the balance of gas exchange in the *Drosophila* nervous system.

Results

Drosophila astrocytes exhibit microdomain Ca^{2+} transients

To monitor the near membrane Ca^{2+} activity in astrocytes, we expressed myristoylated GCaMP5a (myr-GCaMP5a) in astrocytes using the astrocyte-specific *alrm-Gal4* driver (Doherty et al., 2009; Stork et al., 2014). We acutely dissected 3rd instar larval CNS and live-imaged myr-GCaMP5a signals in the ventral nerve cord (VNC)(Ma et al., 2016). We collected images at the midpoint of the neuropil along the dorsoventral axis for 6 minute time windows (Fig 1A). We found that astrocytes exhibited microdomain Ca^{2+} transients that exhibited diverse waveforms, with variable durations and frequencies (Fig 1A). The average full width at half maximum (FWHM) for these Ca^{2+} transients was

5.5±2.26 (mean±SD) seconds (Fig 1B). Microdomain Ca^{2+} transients frequently occurred at the same focus, suggesting there are hotspots where microdomains repeatedly occur for a given astrocyte. The majority of foci exhibited 1-3 events during the 6 minute imaging window (Fig 1C), and Ca^{2+} transients at different sites did not exhibit obvious synchrony. We also found these microdomain Ca^{2+} transients with similar dynamics, although with a slightly shorter duration (FWHM, 1.7±0.08s, mean±SD) in the astrocytes of intact L1 (or 1st instar) larvae (Fig S1A and S1B), suggesting the microdomain Ca^{2+} transients in the acute CNS preparations we observed reflect *in vivo* astrocyte activity. Blockade of action potential firing with tetrodotoxin did not alter astrocyte microdomain Ca^{2+} transients, although they were eliminated by removal of extracellular Ca^{2+} and were sensitive to the Ca^{2+} channel blocker lanthanum chloride (Fig 1D), suggesting Ca^{2+} entry from extracellular space is essential for generation of astrocyte microdomain Ca^{2+} transients.

Astrocytes tile with one another and occupy unique spatial domains in the CNS. We sought to determine whether microdomain Ca^{2+} transients spanned astrocyte-astrocyte cell boundaries, or if they appeared only within the domain of single cells. We used a flippable construct expressing either QF or Gal4 under the control of the *alrm* promoter, along with two genetically encoded Ca^{2+} indicators: *QUAS::myr-GCaMP5a* and *UAS::myr-R-GECO1* (Fig S1C). To confirm both myr-GCaMP5a and myr-R-GECO1 behaved similarily, we first examined double-positive (yellow) cells and found both can detect the same microdomain Ca^{2+} transients (Fig S1D), and in cells exclusively expressing one of these two Ca^{2+} indicators there were no differences in the overall frequency of the microdomain Ca^{2+} events detected (Fig 1E). We then identified cell boundaries between myr-GCaMP5a/myr-R-GECO1-labeled cells, and examined the dynamics of astrocyte microdomains across those boundaries. We observed coincident signaling with myr-GCaMP5a and myr-R-GECO1 (Fig 1E). These data indicate that individual astrocyte microdomain Ca^{2+} transients can span astrocyte-astrocyte borders. Our observations support the notion that astrocyte microdomain Ca^{2+} transients are regulated by extrinsic cues that can simultaneously stimulate two astrocytes, or that astrocyte-astrocyte communication/coupling is sufficient to coordinate very local Ca^{2+} signaling events across neighboring cells.

Astrocyte microdomain Ca^{2+} transients are enhanced by Tyr through TyrRII and mediated by TrpML

To determine whether neurotransmitters were capable of modulating *Drosophila* astrocyte microdomain Ca^{2+} transients, we bath applied several neurotransmitters and live-imaged astrocyte microdomain Ca^{2+} events. Application of glutamate, acetylcholine, GABA, or octopamine had no effect on the frequency of astrocyte microdomain Ca^{2+} transients (Fig 2A). In contrast, application of tyramine led to a significant increase in the frequency of these transients by ~40% (Fig 2A). We screened the known receptors for tyramine in *Drosophila* and found that astrocyte-specific depletion of TyrRII blocked the ability of tyramine to stimulate astrocyte microdomain Ca^{2+} transients (Fig 2A). The spontaneous microdomain events were not dependent on the presence of tyramine or octopamine, as mutants that block the production of tyramine and octopamine (*Tdc2*^{RO54}) or octopamine (*Tβh*^{nM18}) did not significantly alter the frequency of astrocyte microdomain Ca^{2+} transients, nor did mutations in *Oct-TyrR*, which we previously showed was essential for activation of whole-cell Ca^{2+} transients in astrocytes (Fig 2B).

Whole-cell astrocyte transients are regulated by the TRP channel Water witch (Wtrw) (Ma et al., 2016), and astrocyte basal Ca^{2+} levels in mammals modulated by TrpA1 (Shigetomi et al., 2013). We speculated that astrocyte microdomain Ca^{2+} transients might be regulated by one or more of the other 13 TRP channels encoded in the *Drosophila* genome. We screened these for potential roles in the regulation of astrocyte microdomain Ca^{2+} transients by observing Ca^{2+} transients in mutant or astrocyte specific RNAi animals. While 11 of these had no effect, we found that microdomain Ca^{2+} events decrease by ~70% to 80% in *trpml* loss of function mutants, in both intact 1st instar larvae (Fig S1E) and acute CNS preparations from 3rd instar larvae (Fig 2C). Astrocyte specific knockdown of *trpml* also reduced microdomain Ca^{2+} events by ~60% (Fig 2C), arguing for a tissue autonomous role of TrpML in regulating astrocyte microdomain Ca^{2+} transients. Although application of tyramine still increased microdomain Ca^{2+} events in *trpml* mutant backgrounds, the enhancement above the basal level of spontaneous microdomain Ca^{2+} transients was significantly reduced, suggesting that TrpML acts downstream of TyrRII (Fig 2D).

Previous work has shown that reactive oxygen species (ROS) can activate TrpML (Zhang et al., 2016), and astrocyte near membrane Ca^{2+} events are sensitive to ROS in mammals (Agarwal et al., 2017). We therefore assayed the sensitivity of *Drosophila* astrocyte microdomain Ca^{2+} transients to ROS. We observed that bath application of the ROS generator hydrogen peroxide (H_2O_2) led to a TrpML-dependent increase in astrocyte microdomain Ca^{2+} events, while, reciprocally, addition of the antioxidant N-acetyl cysteine completely abolished them (Fig 2E and 2F). These data indicate that astrocyte microdomain Ca^{2+} transients are regulated by tyramine through TyrRII, they are mediated by TrpML and are highly sensitive to ROS. Furthermore, our data demonstrate that astrocyte microdomain Ca^{2+} transients and whole-cell changes in astrocyte Ca^{2+} are physiologically and genetically distinct signaling events.

Astrocyte microdomain Ca^{2+} transients are associated with tracheal branches and precede tracheal filopodia retraction

Trachea are an interconnected series of gas-filled tubes that penetrate insect tissues, are open to the environment, and allow for gas exchange. The inner lining of tracheal tubes are covered by a porous cuticle, which is secreted by the surrounding tracheal cells, and gas exchange is thought to occur through tracheal cell-tissue interactions (Ghabrial et al., 2003). Mammalian astrocytes make intimate contacts with blood vessels by forming endfeet to allow for gas exchange, uptake of nutrients from blood, and maintenance of the blood brain barrier. Tracheal cells share many molecular features during development, morphogenesis and gas exchange with mammalian blood vessels (Ghabrial et al., 2003). The fine processes of *Drosophila* astrocytes are closely associated with the tracheal system (Freeman, 2015). Interestingly, we observed that ~50% of loci where astrocyte microdomain Ca^{2+} events occurred overlapped with tracheal branches in the ventral nerve cord (Fig 3A). In live preparations where trachea were labeled with myristoylated tdTomato (myr-tdTom), actin with Lifeact-GFP, or microtubules with Tubulin-GFP, we observed that tracheal branches dynamically extended and retracted actin-rich protrusions that are characteristic of filopodia (Fig 3B), and only very few were stabilized by microtubules (Fig S2A), implying tracheal branches dynamically explore their surroundings in the CNS with filopodia as they regulate gas

exchange. We next live-imaged tracheal dynamics with myr-tdTom and astrocyte microdomain Ca^{2+} transients simultaneously. To explore the relationship between tracheal filopodial dynamics and astrocyte Ca^{2+} transients, we focused on events where dynamic tracheal filopodia (i.e. those that exhibited both extension and retraction events during the imaging window) and an adjacent astrocyte Ca^{2+} transient were contained in the plane of focus. This represented ~35% (61/174) of all tracheal filopodia that we imaged. Strikingly, we found that astrocyte microdomain Ca^{2+} transients always preceded the retraction of tracheal filopodia (Fig 3C) and that the onset of trachea filopodial retraction was tightly correlated with astrocyte microdomain Ca^{2+} transients (R^2=0.99, Fig 3D-3F), with a latency time of 25.1±0.3s. These observations suggest that astrocyte microdomain Ca^{2+} transients promote the retraction of tracheal filopodial.

Blockade of astrocyte microdomain Ca^{2+} transients increases CNS ROS and *trpML* mutants exhibit increased tracheal growth

We sought to determine whether astrocyte microdomain Ca^{2+} transients regulated tracheal dynamics in the CNS. To block astrocyte microdomain Ca^{2+} transients we used *trpml*^{1} mutants, and labeled tracheal membranes with myr-tdTom. We found in *trpml*^{1} mutant background that while there was no change in the overall rate of tracheal retraction, we observed an increase in the overall rate of tracheal growth over time, which resulted in an increase in maximum length of the tracheal filopodia (Fig 4A). To determine whether stimulating an increased number of astrocyte microdomain Ca^{2+} transients could drive tracheal retraction, we bath applied tyramine. We found tyramine application lead to an increase in the percentage of retracting tracheal filopodia (Fig 4B). To more carefully quantify the effect of loss of *trpml* (and astrocyte microdomain Ca^{2+} transients), we first counted the total number of protrusions from a pair of most posterior ganglion trachea (mpgTr) that innervate a few segments from A5 to A8/9 in the ventral nerve cord. We found that mpgTr in the ventral nerve cord in *trpml*^{1} mutants exhibit increased total length compared to those in control animals (Fig S3). We next examined a uniquely identifiable branch of the tracheal system in the larval optic neuropil (LON). The LON is a simple tissue, composed of only a few dozen neurons and 1~2 tracheal branches that are surrounded by the processes from a single astrocyte (Fig 4C).

Compared to controls, we found that *trpml*^{1} mutants exhibited an approximate doubling of the number of tracheal branches, and also total filopodia in the LON (Fig 4C and S2B).

It is plausible that such an increase in tracheal branches and filopodia might result in excessive O_2 delivery to CNS tissues and result in a hyperoxia. To assay ROS status in the CNS we stained with the ROS indicator dihydroethidium (DHE). In live preparations of *trpml*^{1} mutants we found a ~2.5-fold increase in oxidized DHE^{+} puncta, likely in mitochondria (Bindokas et al., 1996), and when we eliminated *trpml* selectively from astrocytes by RNAi, we found a ~3-fold increase in oxidized DHE^{+} puncta (Fig 4D). These data support the notion that blockade of astrocyte TrpML signaling, and in turn astrocyte microdomain Ca^{2+} transients, leads to increased ROS in the CNS, likely due to increased O_2 delivery from excessive tracheal branches.

Reciprocal interactions between hypoxia-related signaling pathways and astrocyte microdomain Ca^{2+} transients

Hif-1α is a key regulator of tissue responses to changes in oxygen tension. The *Drosophila* homolog of Hif-1α, Similar (Sima), like its mammalian counterpart is hydroxylated and degraded by the proteasome under normoxia (Irisarri et al., 2009; Romero et al., 2008). When tissues become hypoxic, Sima drives the transcription of hypoxia-related genes (Lisy and Peet, 2008). Hif-1α has also been proposed to be important for modulating tissue responses to increased oxygen and ROS (Fratantonio et al., 2018; Movafagh et al., 2015) but this remains somewhat controversial (Jeong et al., 2005; Terraneo et al., 2014). Unexpectedly, we found in *sima* mutants that astrocyte microdomain Ca^{2+} transients were almost completely eliminated (Fig 5A). Astrocyte microdomain Ca^{2+} signaling events are therefore directly or indirectly regulated by this key hypoxia signaling factor. We next attempted to increase tracheal coverage of the CNS by expressing an activated version of the FGF receptor Breathless (λBtl) in trachea using *btl-Gal4*. We sought to determine whether increased tracheal coverage would result in increased astrocyte microdomain Ca^{2+} transients. However, while we found that the total number of large tracheal branches in the CNS was increased by λBtl, examination of tracheal area in single focal planes did not result in enhanced coverage

of CNS tissues by trachea or a significant increase in astrocyte microdomain Ca^{2+} transients (Fig 5B). Tracheal growth is regulated potently by the Branchless (Bnl) FGF, a ligand for Breathless (Ghabrial et al., 2003). To determine whether Bnl might be activated in *trpml* mutants, we examined the expression of a *branchless-LacZ* reporter. Interestingly, we observed increased *bnl-LacZ* expression in *trpml* mutants (Fig 5C), which might partially account for the increased tracheal coverage of the CNS in *trpML* mutants. Together these data identify reciprocal regulatory interactions between Hif-1α, Bnl/FGF signaling, and the astrocyte microdomain Ca^{2+} signaling machinery. That astrocyte microdomain Ca^{2+} signaling is regulated by the key hypoxia factor Hif-1α further supports the notion that astrocyte microdomain Ca^{2+} transients are involved in modulating CNS gas exchange.

Discussion

Molecules required for the generation of astrocyte microdomain Ca^{2+} transients have remained elusive, and the *in vivo* roles for these transients remain controversial and poorly defined (Agarwal et al., 2017; Bazargani and Attwell, 2016). Our work demonstrates that *Drosophila* astrocyte microdomain Ca^{2+} transients share many properties with their mammalian counterparts, are mediated by the TRP channel TrpML, and can be stimulated by ROS and tyramine through the TyrRII receptor. Unexpectedly, we found that they are closely associated with tracheal elements, astrocyte microdomain Ca^{2+} transients precede and are tightly coupled with tracheal filopodial retraction, and that stimulating astrocyte microdomain Ca^{2+} transients with tyramine can promote tracheal filopodial retraction. We propose that modulation of CNS gas exchange through TrpML and ROS signaling represents a key role of astrocyte microdomain Ca^{2+} transients.

Astrocyte microdomain Ca^{2+} transients in *Drosophila* share many features with those observed in mammals (Agarwal et al., 2017; Nett et al., 2002; Srinivasan et al., 2015). They are spontaneously generated, exhibit diverse waveforms, and appear for the most part asynchronous. Their production requires the presence of extracellular Ca^{2+} and they are suppressed by the broad Ca^{2+} channel blocker $LaCl_3$. Our analysis of

adjacent astrocytes that are labeled with uniquely identifiable Ca^{2+} indicators (myr-GCaMP5a versus myr-R-GECO1) demonstrated individual astrocyte microdomain Ca^{2+} transients can span astrocyte-astrocyte boundaries, which might argue for an extrinsic mechanism regulating their production. Alternatively, it might indicate that astrocyte-astrocyte coupling of Ca^{2+} signaling events is strong during their production. Astrocyte microdomain Ca^{2+} transients are not suppressed by blockade of action potentials with tetrodotoxin, suggesting they are not activity dependent, although we also cannot formally rule out a role for spontaneous release of neurotransmitters at synapses. Based on their persistence in *Tdc2* mutants, which lack tyramine and octopamine in CNS, we conclude that spontaneous astrocyte microdomain Ca^{2+} transients do not require the production of tyramine or octopamine *in vivo*. Similar to bath application of norepinephrine in mouse preparations (Agarwal et al., 2017), we found that tyramine was capable of stimulating an increase in astrocyte microdomain Ca^{2+} transients, and that this required the tyramine receptor TyrRII on astrocytes. Why these transients do not require tyramine for their spontaneous production, but can be stimulated by tyramine application, remains unclear. Tyramine can stimulate increases in whole-cell Ca^{2+} levels in astrocytes through the Oct-TyrR, as does octopamine (Ma et al., 2016), but octomapine has no effect in astrocyte microdomain Ca^{2+} transients. It is possible that signaling mediated by TyrRII can somehow increase the open probability of TrpML in microdomains in a way that is distinct from whole-cell Ca^{2+} signaling. This is consistent with our observation that TrpML is partially responsible for the tyramine-induced increase in astrocyte microdomain Ca^{2+} transients.

Astrocyte microdomain Ca^{2+} transients and whole-cell changes in astrocyte Ca^{2+} signaling appear to be distinct, in terms of their regulation by neurotransmitters, the molecular machinery that produces them, and their functional roles (Agarwal et al., 2017; Bazargani and Attwell, 2016; Srinivasan et al., 2015). In mammals, whole-cell astrocyte Ca^{2+} transients are modulated by norepinephrine, adrenergic receptor signaling, and startle stimuli, while microdomain Ca^{2+} transients are associated with mitochondria and are sensitive to ROS (Agarwal et al., 2017). There appears to be a remarkable conservation of both types of astrocyte Ca^{2+} signaling events from mouse to *Drosophila*. Whole-cell transients in flies are activated by tyramine or octopamine (the invertebrate

adrenergic neurotransmitters), which we previously showed activates the Oct-TyrR receptor and the TRP channel Water witch on astrocytes, and in turn through the adenosine receptor AdoR, mediate many of the physiological and behavioral changes exerted by tyramine and octopamine (Ma et al., 2016). The dynamics and regulation of microdomain Ca^{2+} transients are also well-conserved (e.g. regulation by ROS). In the fly they are stimulated by tyramine (but not octopamine), and are mediated by the TRP channel TrpML. In mouse, microdomain Ca^{2+} transients are associated with mitochondria, which have been proposed to serve as a source of ROS, potentially through transient opening of the mPTP (Agarwal et al., 2017). These events may also require mitochondria in *Drosophila*, however the density of mitochondria in astrocyte processes was sufficiently high in our preparations that drawing such a conclusion was not feasible—a single astrocyte microdomain Ca^{2+} transient appears to span domains that include many mitochondria. Nevertheless, it is tempting to speculate that astrocyte microdomain Ca^{2+} transients across species are functionally distinct from whole-cell fluctuations, and play a role predominantly in coupling astrocyte signaling with gas exchange or other dynamic metabolic changes in neural circuits (Agarwal et al., 2017).

Maintaining a healthy, spatiotemporally regulated normoxic environment to prevent either hypoxia or hyperoxia in CNS is a huge challenge, as the O_2-consuming metabolism is thought to fluctuate vigorously in response to neural activity. The close association of astrocyte microdomain Ca^{2+} transients with trachea, the larval breathing apparatus, and with tracheal retractions in particular, suggests a role in modulating CNS gas exchange. Increase in O_2 delivery to tissues can lead to hyperoxia and elevated production of ROS. TrpML has recently been found to be a ROS sensor (Zhang et al., 2016), which would allow for a simple mechanism for ROS-mediated activation of TrpML downstream of increased O_2 delivery. Consistent with such a role in maintenance of gas exchange, we found an increase in ROS in the CNS of *trpml* mutants, and we demonstrated that bath application of tyramine to stimulate astrocyte microdomain Ca^{2+} transients was sufficient to promote tracheal filopodial retraction. Together our data strongly support the notion that TrpML-mediated microdomain Ca^{2+} transients in astrocytes facilitate tracheal retraction, however we cannot exclude the possibility that TrpML might also function in other tissues (e.g. neurons or trachea) in

regulating tracheal dynamics. Surprisingly, we found the transcription factor Sima/Hif-1α, which promotes tracheal growth in response to changing O_2 conditions (Best, 2019), is also required for normal levels of astrocyte microdomain Ca^{2+} transients. It appears that one effect of astrocyte microdomain Ca^{2+} signaling is to feed back to suppress overall tracheal filopodial growth, perhaps thereby lowering O_2 delivery and avoiding hyperoxia. Loss of TrpML led to a clear increase in tracheal growth in neural tissues, which may be partially attributed to the elevated Bnl expression we observed in *trpml* mutants. These observations reveal a mechanistic link between astrocyte Ca^{2+} signaling and key molecular factors that regulate gas exchange throughout metazoan tissues (Fig 5D). Based on our findings, we propose astrocyte microdomain Ca^{2+} transients in the larval CNS coordinate gas exchange through regulation of tracheal dynamics, thereby balancing O_2 delivery/CO_2 removal according to local metabolic needs.

Figure Legends

Figure 1. Characterization of microdomain Ca^{2+} transients in *Drosophila* astrocytes.

(A) Schematic of larval CNS (light gray, neuropil; gray, cortex). An imaging area showing membrane tethered myr-GCaMP5a expression driven by *alrm-Gal4* in astrocytes, in which microdomain Ca^{2+} transients during 6min were maximally projected (in pseudocolor, grayscale values ranging from 0 to 255. scale bar, 20µm). Representative time-lapse images of microdomain Ca^{2+} transients in 2 ROIs (1, 2). Traces of microdomain Ca^{2+} transients in 8 ROIs (a-h) over 6 min.

(B) Superimposed traces of individual microdomain Ca^{2+} transients and an average with its full width at half maximum (FWHM, mean±SD).

(C) Histogram showing the distribution of recurrent microdomain Ca^{2+} transients at same foci.

(D) Responses of microdomain Ca^{2+} transients to tetrodotoxin, zero extracellular Ca^{2+} and $LaCl_3$ (n=6, mean±SEM, one-way ANOVA).

(E) 2-color Ca^{2+} imaging in neighboring astrocytes. In presence of the flippase repo-FLP, myr-GCaMP5a (green) expressing astrocytes switch to express myr-R-GECO1 (red), resulting in 3 types of astrocytes expressing both (yellow) or either one of these 2 Ca^{2+} indicators (scale bar, 20µm). Time-lapse images and superimposed traces of representative microdomain Ca^{2+} transients at 2 juxtaposed ROIs between myr-GCaMP5a and myr-R-GECO1 expressing astrocytes. Quantification is from Ca^{2+} imaging of myr-GCaMP5a and myr-R-GECO1 that were exclusively expressed in different astrocytes.

Figure 2. Astrocyte microdomain Ca^{2+} transients are genetically distinct from soma transients and require TrpML.

(A) Responses of microdomain Ca^{2+} transients to neurotransmitters/neuromodulators in presence of tetrodotoxin (n=6, mean±SEM, paired t-test). Left panel, control preparations; right panel, gentypes as indicated.

(B) Quantification of microdomain Ca^{2+} transients in *Tdc2*^{RO54}, *Tβh*^{nM18} or *Oct-TyrR*^{hono} mutants (n=6, mean±SEM, one-way ANOVA).

(C) Maximal projected astrocyte microdomain Ca^{2+} transients during 6min in control, *trpml*^{1} mutants, and astrocyte-specific *trpml*^{RNAi} (in pseudocolor, grayscale values ranging from 0 to 255. scale bar, 20µm). Quantification of microdomain Ca^{2+} transients in mutants (loss-of-function mutations or astrocyte specific RNAi driven by *alrm-Gal4*) of genes encoding TRP family ion channels (n=6, mean±SEM, one-way ANOVA).

(D) Effects of tyramine treatment on controls and *trpml*^{1} mutants (n=6, mean±SEM, one-way ANOVA. within groups, paired t-test). Right panel, increase in transients by tyramine (subtracting basal included) in control and *trpml*^{1} mutants.

(E and F) H_2O_2, antioxidant N-acetyl cysteine (NAC) treatments of larval CNS (n=6, mean±SEM, one-way ANOVA. within groups, paired t-test). -, + indicate pre-, post-delivery of the chemicals tested.

Figure 3. Astrocyte microdomain Ca^{2+} transients are close to tracheal branches and precede retraction of tracheal filopodia.

(A) Astrocyte microdomain Ca^{2+} transients (green) overlap with tracheal branches (red) (scale bar, 20µm).

(B) Tracheal branches extend and retract F-actin containing filopodia. Asterisks, myr-tdTomato labeled filopodia; Arrows, Lifeact-GFP labeled F-actin (scale bar, 10µm).

(C) Time-lapse images and superimposed traces (green trace, myr-GCaMP5a in astrocytes expressed as dF/F0; red trace, myr-tdTomato in tracheal filopodia expressed as length) of 3 pairs (p1, p2, p3) of tracheal filapodia and astrocyte microdomain Ca^{2+} transients (scale bar, 10µm). Blue boxes represent time windows where tracheal filapodia have grown into astrocyte microdomain Ca^{2+} transients space. Note that prior to entering the astrocyte Ca^{2+} microdomain, tracheal filapodial retraction is not coupled to increases in astrocyte Ca^{2+}, but after entry, increased astrocyte Ca^{2+} is strongly correlated with tracheal filapodial retraction.

(D) Temporal correlation between onset of filopodia retraction and timing of peak astrocyte microdomain Ca^{2+} transients in seconds (n=61 dynamic filopodia).

(E) Distribution of onset of filopodial extention or retraction events relative to astrocyte microdomain Ca^{2+} peak.

(F) Time interval between astrocyte microdomain Ca^{2+} transients and tracheal filopodial growth versus retraction. Onset of extension time is broadly distributed relative to the peak astrocyte Ca^{2+} signal, while the timing of peak retraction is tightly correlated with peak astrocyte Ca^{2+} transient.

Figure 4. Loss of TrpML leads to overgrowth of trachea and excessive reactive oxygen species (ROS) in larval CNS.

(A) Quantification of overall filopodial retraction and extension rates, and maximal length of tracheal filopodia (mean±SEM, t-test).

(B) Comparison of rates of tracheal filopodial extension and retraction in control and *trpml*^{1} mutants, and changes in extension retractions ratios after bath application of tyramine (n=6, mean±SEM, one-way ANOVA. within groups, paired t-test).

(C) Schematic of larval optic neuropil (LON). ap, astrocyte process; tb, tracheal branch; tf, tracheal filopodium. In control, one tracheal branch (labeled with *btl>myr::tdTom*, arrowhead) near the LON (Brp, blue) grows short filopodia (arrows) into the LON. In

trpml^{1}, two transverse tracheal branches grow near the LON, and they exhibit increases in filopodial extension into the LON (n=20, mean±SEM, t-test. scale bar, 10µm).

(D) Dihydroethidium (DHE) staining in indicated genotypes. NAC was added 5 min prior to DHE incubation. DHE oxidized by ROS to form 2-hydroxyethidium (2-OH-E^{+}) and ethidium (E^{+}). Quatifications to right (n=6, mean±SEM, t-test. scale bar, 50µm).

Figure 5. Astrocyte microdomain Ca^{2+} transients require Sima, and Bnl expression is increased in *trpML* mutants.

(A) Astrocyte microdomain Ca^{2+} transients in *sima* mutants or after *sima* expression in trachea (n=6, t-test).

(B) Z-projection of tracheal branches (labeled with *btl>myr::tdTom*) in ventral nerve cords after *λbtl* expression in trachea; quantification of number of major tracheal branches in Z projection and coverage area in single focal planes; and quantification astrocyte microdomain Ca^{2+} transients (n=6, mean±SEM, t-test. scale bar, 40µm). Genotypes as indicated.

(C) Ventral nerve cord expression of *bnl-LacZ* expression in controls and *trpml*^{1} mutants (n=6, t-test).

(D) Proposed model. Astrocyte microdomain Ca^{2+} transients modulated by reactive oxygen species (ROS) and TrpML facilitate filopodia retraction. Cell membrane or lysosomal localization of TrpML regulates Ca^{2+} signaling in response to ROS to generate astrocyte microdomain Ca^{2+} transients. Tyramine induces increased microdomain Ca^{2+} transients by activating TrpML. Increased or decreased astrocyte Ca^{2+} signaling modulates tracheal retraction or growth, respectively. Sima signaling controls levels of astrocyte Ca^{2+} signaling, and changes in astrocyte signaling resulting from TrpML loss feedback on Bnl expression.

Figure S1. Spontaneous astrocyte microdomain Ca^{2+} transients in intact larvae.

(A) Astrocytes expressing myr-GCaMP5a in the ventral nerve cord of 1st instar larvae. Traces of 8 representative microdomain Ca^{2+} transients.

(B) Superimposed traces of individual microdomain Ca^{2+} transients and an average.

(C) Schematic of inducing 2-color Ca^{2+} indicators mosaic expression in neighboring astrocytes (green, red, yellow).

(D) 2 representative microdomain Ca^{2+} transients in dual myr-GCaMP5a/myr-R-GECO1 astrocytes. Note that both myr-GCaMP5a and myr-R-GECO1 exhibit similar dynamics when in the same astrocyte.

(E) Quantification of microdomain Ca^{2+} transients in control and *trpml*^{1} mutant in intact 1st instar larvae (n=6, mean±SEM, t-test.).

Figure S2. Distribution of microtubules and F-actin in larval CNS trachea.

(A) Tracheal branches were visualized using myr-tdTomato and cytoskeletal elements were visualized with: microtubles (αTub-GFP) and F-actin (Lifeact-GFP). Microtubules were present in major tracheal branches but were found in only a few membrane protrusions (arrow), the majority were unlabeled (asterisks). F-actin was found to be present in all tracheal membrane protrusions (dotted boxes).

(B) Representative images of larval brains showing the position of LONs (dashed boxes). Image represents an 8.1µm projection, covering brain neuropil and LONs (blue) and associated tracheal branches/filopodia. LONs zoomed in Fig 4C.

Figure S3. Tracheal branches overgrow in the larval ventral nerve cord of *trpml*^{1} mutants.

Tracheal autofluorescence when illuminated with a 408nm laser was used to trace individual branches sprouting from the pair of mpgTr (red arrows). The ventral nerve cords are outlined with red dashed lines (n=8-10, mean±SEM, t-test).

Key source table

REAGENTS OR RESOURCE	SOURCE	IDENTIFIER
Fly strains		
trpml^{1}	Bloomington Stock Center	28992
trpml^{2}	Bloomington Stock Center	42230
trpml^{JF01239}	Bloomington Stock Center	31294
tyrR^{JF01878}	Bloomington Stock Center	25857
tyrRII^{JF02749}	Bloomington Stock Center	27670
trpA1^{1}	Bloomington Stock Center	36342
trpm^{2}	Bloomington Stock Center	35527
nompC^{3}	Bloomington Stock Center	42258
trp^{1}	Bloomington Stock Center	5692
trpl^{302}	Bloomington Stock Center	31433
pkd2^{1}	Bloomington Stock Center	24495
trpγ^{JF01244}	Bloomington Stock Center	31299
pyx^{JF01242}	Bloomington Stock Center	31297
btl-Gal4	Bloomington Stock Center	8807
UAS-Lifeact-GFP	Bloomington Stock Center	57326
UASp-αTub-GFP	Bloomington Stock Center	7373
10XUAS-IVS-myr::tdTomato	Bloomington Stock Center	32222
sima^{07607}	Bloomington Stock Center	14640
UAS-sima	Bloomington Stock Center	9582
UAS-λbtl	Bloomington Stock Center	29045
bnl-lacZ	Bloomington Stock Center	11704
Oct-TyrR^{hono}	Kyoto Stock Center	109038
nompC^{4}	Walker et al., 2000	N/A
painless^{70}	Im et al., 2015	N/A
nan^{36a}	Kim et al., 2003	N/A
wtrw^{ex}	Kim et al., 2010	N/A
Tdc2^{RO54}	Cole et al., 2005	N/A
Tβh^{nM18}	Monastirioti et al., 1996	N/A
alrm-Gal4	Doherty et al., 2009	N/A
alrm>QF>Gal4	Stork et al., 2014	N/A
repo-FLPase	Stork et al., 2014	N/A
alrm-LexA::GAD	Stork et al., 2014	N/A
UAS-myr::GCaMP5a	This paper	N/A

UAS-myr::R-GECO1	This paper	N/A
QUAS-myr::GCaMP5a	This paper	N/A
13XLexAop2-myr::GCaMP6s	This paper	N/A
Antibody		
mouse anti-Brp	DSHB	Cat# nc82
mouse anti-LacZ	Promega	Cat# Z378B
Chemicals		
tetrodotoxin	Tocris	Cat# 1078
lanthanum chloride	Sigma-Aldrich	Cat# 211605
acetylcholine	Sigma-Aldrich	Cat# A6625
γ-aminobutyric acid (GABA)	Sigma-Aldrich	Cat# A2129
glutamate	Sigma-Aldrich	Cat# G1626
tyramine	Sigma-Aldrich	Cat# T90344
octopamine	Sigma-Aldrich	Cat# O0250
N-acetyl cysteine	Sigma-Aldrich	Cat# A7250
hydrogen peroxide	Sigma-Aldrich	Cat# H1009
halocarbon oil 27	Sigma-Aldrich	Cat# H8773
Recombinat DNA		
pUAST-myr::GCaMP5a	This paper	N/A
pQUAST-myr::GCaMP5a	This paper	N/A
pUAST-myr::R-GECO1	This paper	N/A
pJFRC19-13XLexAop2-IVS-myr::GCaMP6s	This paper	N/A
Software		
Volocity	PerkinElmer, Inc.	http://www.perkinelmer.com/lab-products-and-services/cellular-imaging/performing-advanced-image-data-analysis.html
Slidebook	Intelligent Imaging Innovations, Inc.	https://www.intelligent-imaging.com/slidebook
Fiji		https://fiji.sc/
Graphpad Prism 7	GraphPad Software	https://www.graphpad.com/scientific-software/prism/
Igor Pro	WaveMetrics, Inc.	https://www.wavemetrics.com/products/igorpro

Lead Contact and Materials Availability

Further information and requests for resource and reagents should be directed to and will be fulfilled by the Lead Contact, Marc R. Freeman (freemmar@ohsu.edu). All

unique/stable reagents generated in this study are available upon reasonable request from the Lead Contact.

Experimental Model and Subject Details

All larvae/flies were cultured in cornmeal food at 25 ℃ under 12 hour/12 hour dark/light cycles. The specific developmental stages studied in each experiment are indicated in the following Method Details. Female larvae were used for all experiments. Complete genotypes used in each experiment can be found in the Key Resources Table.

Method Details

Constructs and transgenic flies

The full-length ORFs of GCaMP5a, R-GECO1, GCaMP6s with an in-frame DNA fragment encoding the myristoylation signal peptide at 5'-end were cloned into vectors pUAST, pQUAST, pJFRC19 (harboring *13XLexAop2-IVS*, referring to the Addgene plasmid Cat# 26224) to generate constructs *pUAST-myr::GCaMP5a*, *pQUAST-myr::GCaMP5a*, *pUAST-myr::R-GECO1*, *pJFRC19-13XLexAop2-IVS-myr::GCaMP6s* for injection. The transgenic flies were injected and recovered by Rainbow Transgenic Flies, Inc. (California).

Ca^{2+} imaging and data analysis

Ca^{2+} imaging in intact larvae: the 1st instar larva (25℃, 24-32 hours after egg laying) was sandwiched in 30µl halocarbon oil 27 between a slide and a 22 X 22mm coverslip (Cat# 1404-15, Globe Scientific Inc.), then a 3min time-lapse video was taken immediately on a spinning disk confocal microscope equipped with a 40X oil immersion objective.

The CNS dissection from early 3rd instar larvae (larval density ~100, 25℃, 76-84 hours after egg laying) was performed in the imaging buffer (pH7.2) containing 110mM NaCl, 5.4mM KCl, 0.3mM $CaCl_2$, 0.8mM $MgCl_2$, 10mM D-glucose, 10mM HEPES, the CNS was immediately transferred to a silicone coated petri dish, immersed in 100µl imaging buffer (1.2mM $CaCl_2$), and immobilized gently by sticking the attached nerves onto the silicone surface with forceps. The petri dish then was placed on the stage of a spinning disk confocal microscope equipped with a 40X water dipping objective. The focal plane

was fixed around where most of the dorsal lateral astrocytes start to appear in the field of view. After 4min acclimation and stabilization, a 6min movie (excitation channel, 488nm. exposure time, 300ms. single focal plane) was taken for analysis. The 488nm and 516nm channels were alternated for imaging both the microdomain Ca^{2+} transients in astrocytes and the dynamics of tracheal filopodia. To keep the tracheal filopodia in focus during the course of extension and retraction, images spanning 5µM in z depth were taken. For analyzing astrocyte microdomain Ca^{2+} transients-tracheal filopodia interaction, those events that meet the following 2 criteria during imaging were selected: 1) filopodia progress through the entire cycle of budding at tracheal branches, growing, and withdrawing and 2) astrocyte Ca^{2+} transients overlap with those filopodia. The main goal of this analysis was to determine whether there is a correlation between the occurrence of astrocyte transient peaks and the onset of retraction of filopodia.

For bath application of drugs, halfway through the 6min imaging window (~ 3min), 100µl imaging buffer (1.2mM Ca^{2+}) containing drugs (2X final concentration) was directly applied onto the preparations, then imaging continued for another 3min.

The chemicals used for bath application experiments include: tetrodotoxin (1µM), lanthanum chloride ($LaCl_3$), acetylcholine (2.5mM), γ-aminobutyric acid (GABA, 2.5mM), glutamate (2.5mM), tyramine (2.5mM), octopamine (2.5mM), N-acetyl cysteine (NAC, 2.5mM), hydrogen peroxide (H_2O_2, 0.1mM).

The intensity of microdomain Ca^{2+} transients was measured with software Volocity (PerkinElmer, Inc.), and the amplitude of microdomain Ca^{2+} transients was defined by $(F_t-F_0)/F_0$ (t=0,1,2…40, the peak amplitude was designated at t=20) as percentage.

The frequency (the number of microdomain Ca^{2+} transients per minute) of microdomain Ca^{2+} transients in each preparation was quantified as follows: a 100µm X 100µm window was cropped from each movie and resulted in 9 smaller, side-to-side 100pixel X 100pixel windows (line drawing over movies) in which the number of microdomain Ca^{2+} transients was counted manually. The total number of microdomain Ca^{2+} transients in each preparation (100µm X 100µm) was acquired by adding up all the numbers counted in these 9 100pixel X 100pixel windows. The cutoff for defining a Ca^{2+} transient is ~5%

change in delta F/F_0, which is evaluated by *post hoc* calculations after manually selecting active events.

Immunostaining and tracheal branch tracing

The CNS dissected in PBS from 3rd instar larvae (larval density ~100, 25℃, 100-108 hours after egg laying) was immediately transferred in 4% formaldehyde for fixation for 20min (for co-staining with tracheal filopodia, the dissection was performed in the imaging buffer with 0.3mM Ca^{2+}, and the CNS preparations were incubated in the imaging buffer with 1.2mM Ca^{2+} for 10min before 4% formaldehyde fixation). Washing in PBS for 3X 10min. Permeabilization in PBS + 0.3% Triton X-100 for 2 hours. Primary antibody (nc82 1:50 or anti-LacZ 1:500 in PBS + 0.1% Triton X-100) incubation at 4 ℃ for ~72 hours. Secondary antibody incubation at room temperature for ~2 hours.

Under the circumstances we didn't use *btl>myr-tdTom* to visualize trachea, tracheal branches in ventral nerve cord were illuminated with 408nm laser light and emitting autofluorescence was imaged. Each individual branch was then traced manually with Simple Neurite Tracer (Fiji).

Reactive oxygen species detection by DHE (dihydroethidium) staining

The CNS preparations from 3rd instar larvae (larval density ~100, 25℃, 100-108 hours after egg laying) were made exactly in the same way for Ca^{2+} imaging. Incubation in 100µl imaging buffer (1.2mM Ca^{2+}) containing 30µM DHE for 8min before imaging (30µm in z depth, starting from the very dorsal side, was taken). The puncta were automatically counted by segmentation in Slidebook.

Statistics

Comparison between groups was tested by one-way ANOVA with *post hoc* tests, or unpaired t-test. Comparison within groups was tested by paired t-test. $p<0.05$ was considered statistically significant. * $p<0.05$, ** $p<0.01$.

Data and Code Availability

The datasets supporting the current study have not been deposited in a public repository due to file size constraints but are available from the corresponding author on request.

Acknowledgments

We thank Bloomington Stock Center, Kyoto Stock Center, Drs. C.S. Zuker, C. Montell, J. Hirsh and M. Monastirioti for providing flies. We thank A. Sheehan for making constructs. We thank Freeman lab members for feedback on the manuscript.

Author Contributions

Z.G.M., M.R.F. conceived experiments, wrote the manuscript. Z.G.M. performed experiments, analyzed data.

Declaration of Interests

The authors declare no competing interests.

References

Agarwal, A., Wu, P.-H., Hughes, E.G., Fukaya, M., Tischfield, M.A., Langseth, A.J., Wirtz, D., Bergles, D.E., 2017. Transient Opening of the Mitochondrial Permeability Transition Pore Induces Microdomain Calcium Transients in Astrocyte Processes. Neuron 93, 587–605.e7. doi:10.1016/j.neuron.2016.12.034

Bazargani, N., Attwell, D., 2016. Astrocyte calcium signaling: the third wave. Nat. Neurosci. 19, 182–189. doi:10.1038/nn.4201

Best, B.T., 2019. Single-cell branching morphogenesis in the Drosophila trachea. Dev. Biol. 451, 5–15. doi:10.1016/j.ydbio.2018.12.001

Bindokas, V.P., Jordán, J., Lee, C.C., Miller, R.J., 1996. Superoxide production in rat hippocampal neurons: selective imaging with hydroethidine. J. Neurosci. 16, 1324–1336. doi:10.1523/JNEUROSCI.16-04-01324.1996

Ding, F., O'Donnell, J., Thrane, A.S., Zeppenfeld, D., Kang, H., Xie, L., Wang, F., Nedergaard, M., 2013. α1-Adrenergic receptors mediate coordinated Ca2+ signaling of cortical astrocytes in awake, behaving mice. Cell Calcium 54, 387–394. doi:10.1016/j.ceca.2013.09.001

Doherty, J., Logan, M.A., Taşdemir, O.E., Freeman, M.R., 2009. Ensheathing glia function as phagocytes in the adult Drosophila brain. J. Neurosci. 29, 4768–4781. doi:10.1523/JNEUROSCI.5951-08.2009

Fratantonio, D., Cimino, F., Speciale, A., Virgili, F., 2018. Need (more than) two to Tango: Multiple tools to adapt to changes in oxygen availability. Biofactors 44, 207–218. doi:10.1002/biof.1419

Freeman, M.R., 2015. Drosophila Central Nervous System Glia. Cold Spring Harb Perspect Biol a020552. doi:10.1101/cshperspect.a020552

Ghabrial, A., Luschnig, S., Metzstein, M.M., Krasnow, M.A., 2003. Branching morphogenesis of the Drosophila tracheal system. Annu. Rev. Cell Dev. Biol. 19, 623–647. doi:10.1146/annurev.cellbio.19.031403.160043

Irisarri, M., Lavista-Llanos, S., Romero, N.M., Centanin, L., Dekanty, A., Wappner, P., 2009. Central role of the oxygen-dependent degradation domain of Drosophila HIFalpha/Sima in oxygen-dependent nuclear export. Mol. Biol. Cell 20, 3878–3887. doi:10.1091/mbc.e09-01-0038

Jeong, H.-J., Hong, S.-H., Park, R.-K., Shin, T., An, N.-H., Kim, H.-M., 2005. Hypoxia-induced IL-6 production is associated with activation of MAP kinase, HIF-1, and NF-kappaB on HEI-OC1 cells. Hear. Res. 207, 59–67. doi:10.1016/j.heares.2005.04.003

Khakh, B.S., McCarthy, K.D., 2015. Astrocyte Calcium Signaling: From Observations to Functions and the Challenges Therein. Cold Spring Harb Perspect Biol 7, a020404. doi:10.1101/cshperspect.a020404

Lisy, K., Peet, D.J., 2008. Turn me on: regulating HIF transcriptional activity. Cell Death Differ. 15, 642–649. doi:10.1038/sj.cdd.4402315

Ma, Z., Stork, T., Bergles, D.E., Freeman, M.R., 2016. Neuromodulators signal through astrocytes to alter neural circuit activity and behaviour. Nature 539, 428–432. doi:10.1038/nature20145

Movafagh, S., Crook, S., Vo, K., 2015. Regulation of hypoxia-inducible factor-1a by

reactive oxygen species: new developments in an old debate. J. Cell. Biochem. 116, 696–703. doi:10.1002/jcb.25074

Nett, W.J., Oloff, S.H., McCarthy, K.D., 2002. Hippocampal astrocytes in situ exhibit calcium oscillations that occur independent of neuronal activity. J. Neurophysiol. 87, 528–537.

Paukert, M., Agarwal, A., Cha, J., Doze, V.A., Kang, J.U., Bergles, D.E., 2014. Norepinephrine controls astroglial responsiveness to local circuit activity. Neuron 82, 1263–1270. doi:10.1016/j.neuron.2014.04.038

Romero, N.M., Irisarri, M., Roth, P., Cauerhff, A., Samakovlis, C., Wappner, P., 2008. Regulation of the Drosophila hypoxia-inducible factor alpha Sima by CRM1-dependent nuclear export. Mol. Cell. Biol. 28, 3410–3423. doi:10.1128/MCB.01027-07

Rungta, R.L., Bernier, L.-P., Dissing-Olesen, L., Groten, C.J., LeDue, J.M., Ko, R., Drissler, S., MacVicar, B.A., 2016. Ca2+ transients in astrocyte fine processes occur via Ca2+ influx in the adult mouse hippocampus. Glia 64, 2093–2103. doi:10.1002/glia.23042

Shigetomi, E., Jackson-Weaver, O., Huckstepp, R.T., O'Dell, T.J., Khakh, B.S., 2013. TRPA1 channels are regulators of astrocyte basal calcium levels and long-term potentiation via constitutive D-serine release. J. Neurosci. 33, 10143–10153. doi:10.1523/JNEUROSCI.5779-12.2013

Shigetomi, E., Tong, X., Kwan, K.Y., Corey, D.P., Khakh, B.S., 2012. TRPA1 channels regulate astrocyte resting calcium and inhibitory synapse efficacy through GAT-3. Nat. Neurosci. 15, 70–80. doi:10.1038/nn.3000

Srinivasan, R., Huang, B.S., Venugopal, S., Johnston, A.D., Chai, H., Zeng, H., Golshani, P., Khakh, B.S., 2015. Ca(2+) signaling in astrocytes from Ip3r2(-/-) mice in brain slices and during startle responses in vivo. Nat. Neurosci. 18, 708–717. doi:10.1038/nn.4001

Stork, T., Sheehan, A., Tasdemir-Yilmaz, O.E., Freeman, M.R., 2014. Neuron-glia interactions through the Heartless FGF receptor signaling pathway mediate morphogenesis of Drosophila astrocytes. Neuron 83, 388–403. doi:10.1016/j.neuron.2014.06.026

Terraneo, L., Virgili, E., Caretti, A., Bianciardi, P., Samaja, M., 2014. In vivo hyperoxia induces hypoxia-inducible factor-1α overexpression in LNCaP tumors without affecting the tumor growth rate. Int. J. Biochem. Cell Biol. 51, 65–74. doi:10.1016/j.biocel.2014.03.019

Zhang, X., Cheng, X., Yu, L., Yang, J., Calvo, R., Patnaik, S., Hu, X., Gao, Q., Yang, M., Lawas, M., Delling, M., Marugan, J., Ferrer, M., Xu, H., 2016. MCOLN1 is a ROS sensor in lysosomes that regulates autophagy. Nat Commun 7, 12109. doi:10.1038/ncomms12109

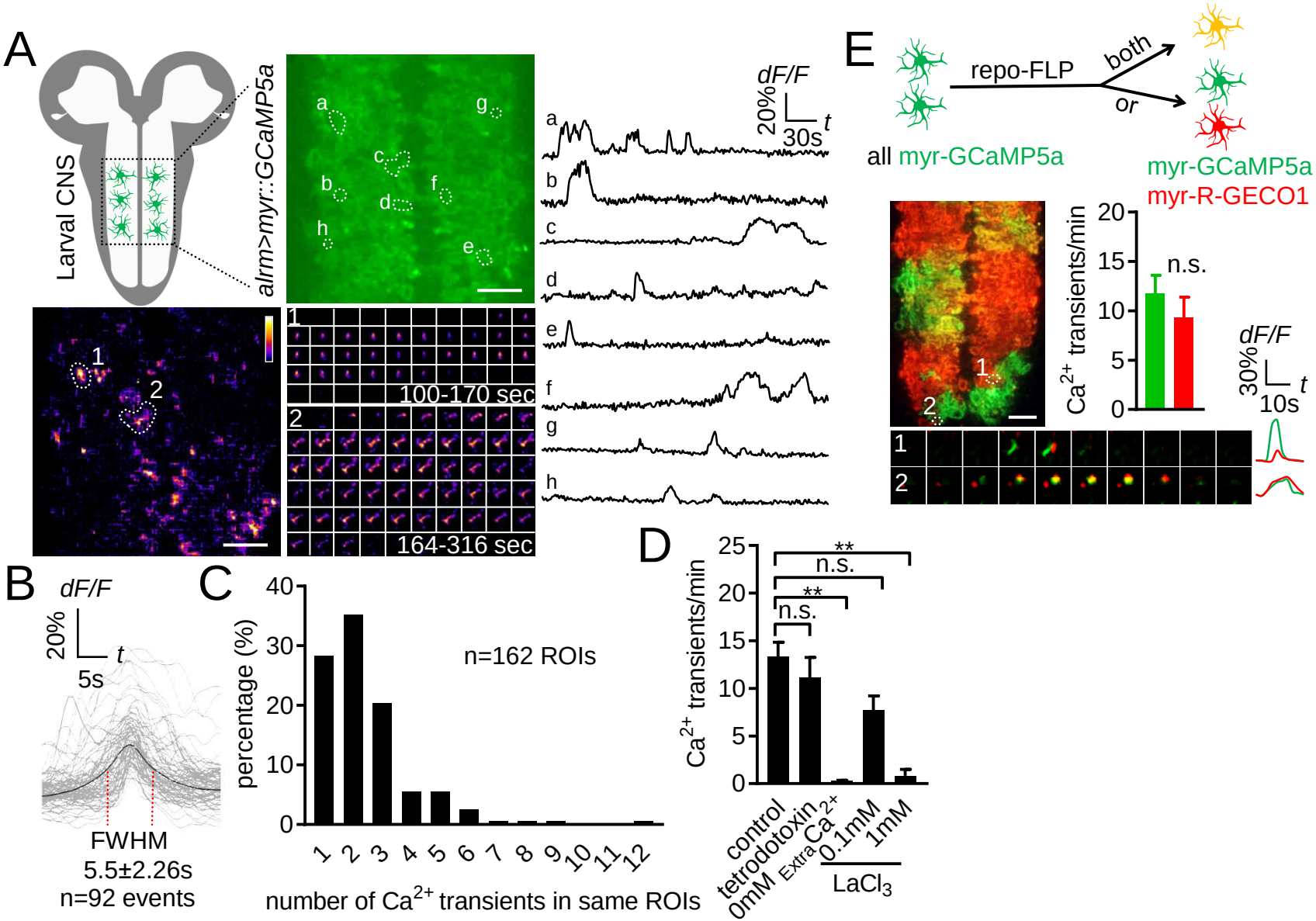
A
Larval CNS
alrm>myr::GCaMP5a
a
b
c
d
e
f
g
h
1
2
100-170 sec
164-316 sec
dF/F
20%
30s
t
B
dF/F
20%
5s
t
FWHM
5.5±2.26s
n=92 events
C
percentage (%)
n=162 ROIs
number of Ca2+ transients in same ROIs
D
Ca2+ transients/min
n.s.
**
control
tetrodotoxin
0mM Extra Ca2+
0.1mM
1mM
LaCl3
E
repo-FLP
both
or
all myr-GCaMP5a
myr-GCaMP5a
myr-R-GECO1
Ca2+ transients/min
n.s.
dF/F
30%
10s
t

Fig 1.

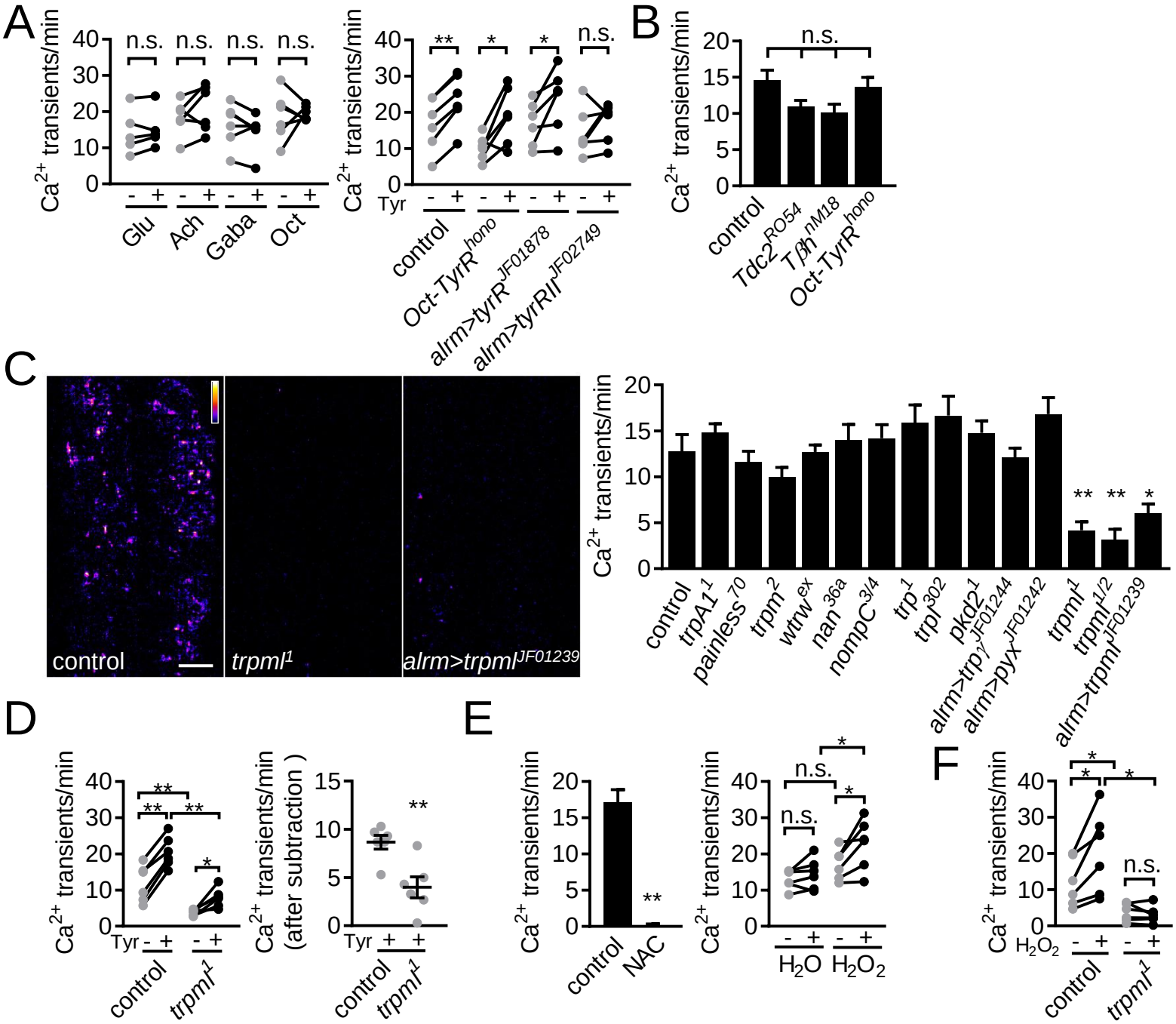
A
Ca2+ transients/min
n.s.
Glu
Ach
Gaba
Oct
Tyr
control
Oct-TyrR hono
alrm>tyrR JF01878
alrm>tyrRII JF02749
B
Tdc2 RO54
Tβh nM18
C
control
trpml1
alrm>trpml JF01239
trpA1 1
painless 70
trpm 2
wtrw ex
nan 36a
nompC 3/4
trp 1
trpl 302
pkd2 1
alrm>trpγ JF01244
alrm>pyx JF01242
trpml 1/2
D
(after subtraction)
E
NAC
H2O
H2O2
F

Fig 2.

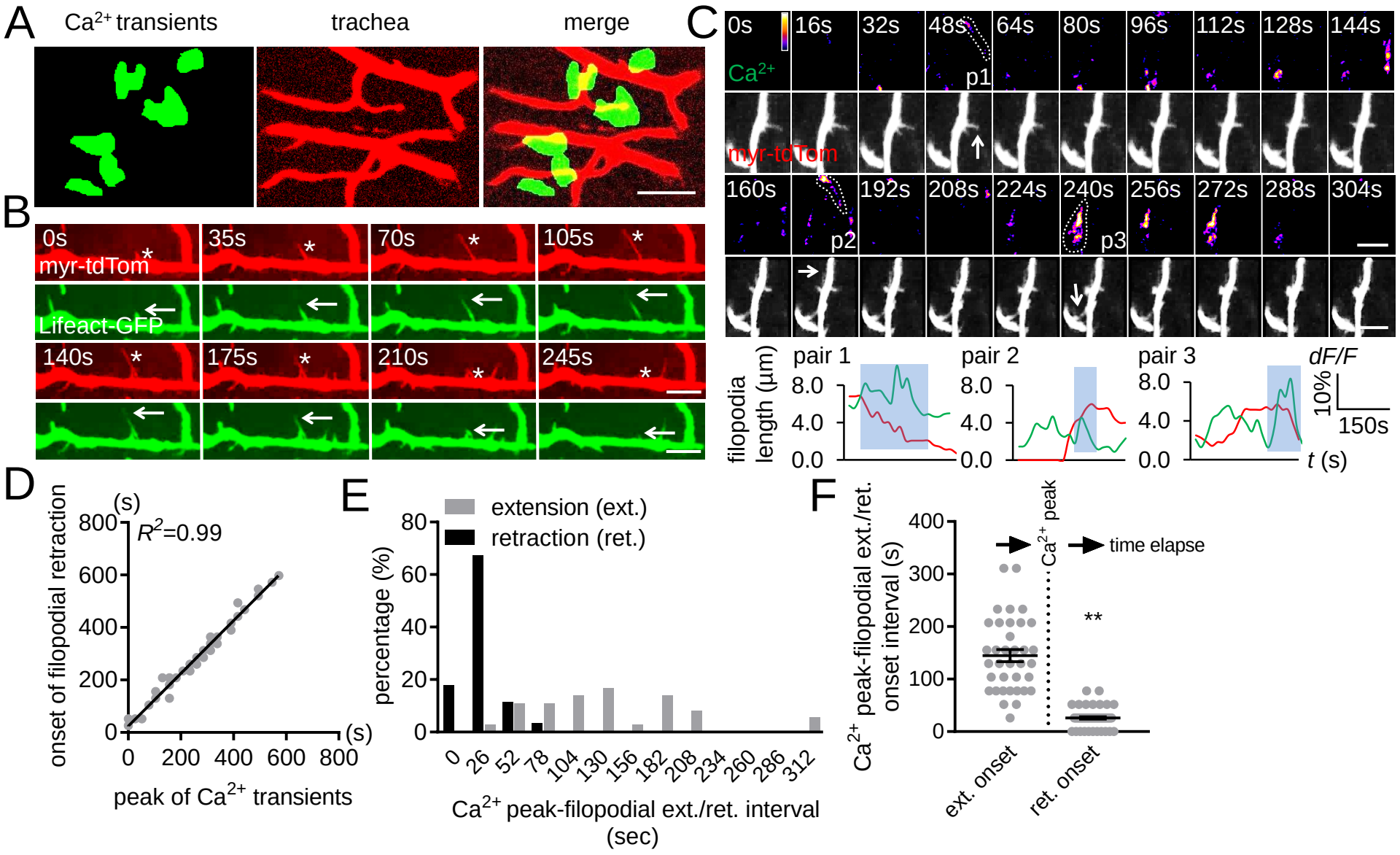
A
Ca2+ transients
trachea
merge
B
0s
35s
70s
105s
myr-tdTom
Lifeact-GFP
140s
175s
210s
245s
C
0s
16s
32s
48s
64s
80s
96s
112s
128s
144s
Ca2+
p1
myr-tdTom
160s
192s
208s
224s
240s
256s
272s
288s
304s
p2
p3
filopodia length (μm)
pair 1
pair 2
pair 3
8.0
4.0
0.0
dF/F
10%
150s
t (s)
D
(s)
R2=0.99
onset of filopodial retraction
peak of Ca2+ transients
E
extension (ext.)
retraction (ret.)
percentage (%)
Ca2+ peak-filopodial ext./ret. interval (sec)
F
Ca2+ peak-filopodial ext./ret. onset interval (s)
Ca2+ peak
time elapse
**
ext. onset
ret. onset

Fig 3.

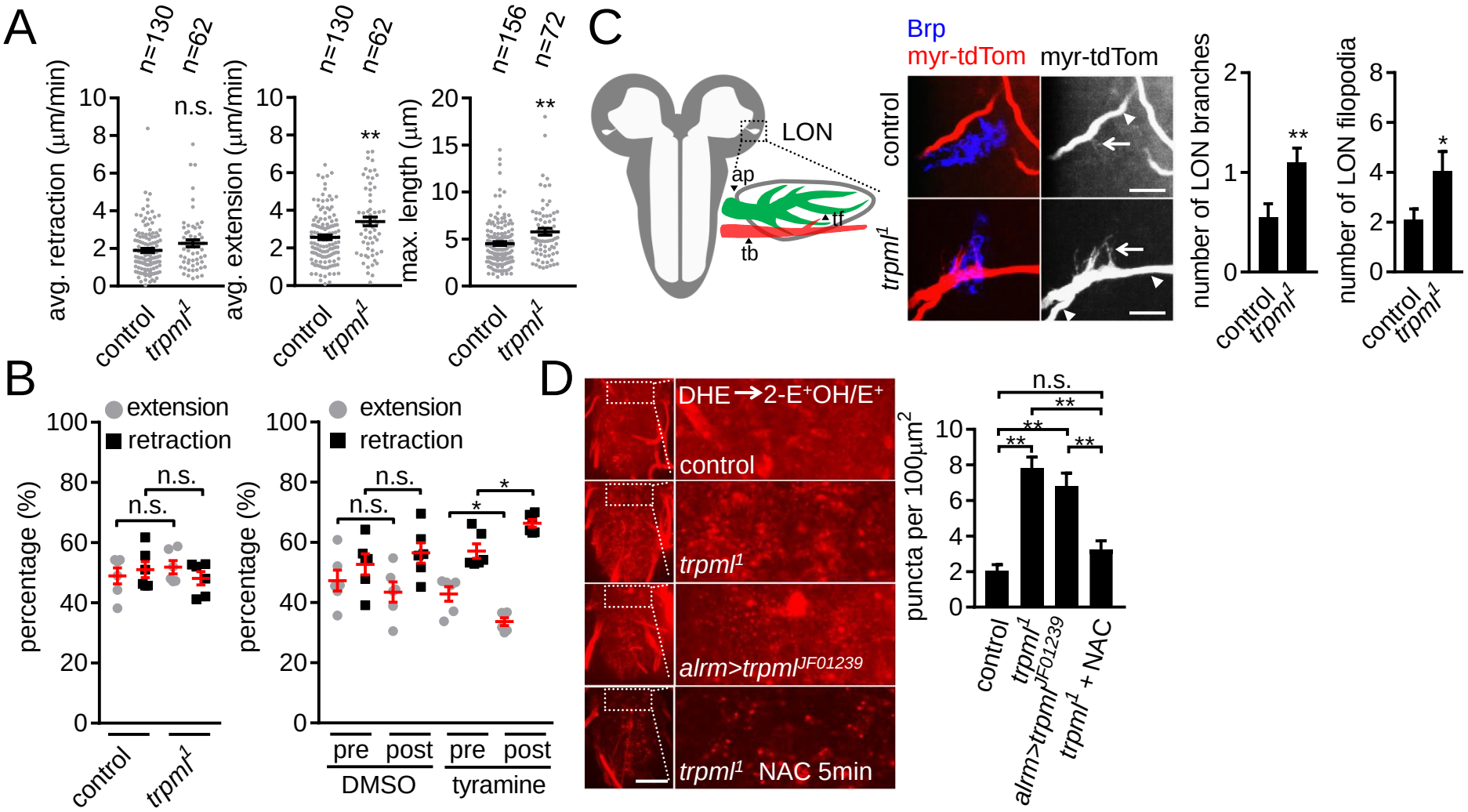
A
n=130
n=62
n=130
n=62
n=156
n=72
avg. retraction (μm/min)
avg. extension (μm/min)
max. length (μm)
n.s.
**
**
control
trpml1
B
extension
retraction
percentage (%)
n.s.
n.s.
n.s.
n.s.
*
*
pre
post
pre
post
DMSO
tyramine
C
LON
ap
tf
tb
Brp
myr-tdTom
myr-tdTom
number of LON branches
number of LON filopodia
**
*
D
DHE→2-E+OH/E+
control
trpml1
alrm>trpmlJF01239
trpml1 NAC 5min
puncta per 100μm2
n.s.
**
**
**
**
control
trpml1
alrm>trpmlJF01239
trpml1 + NAC

Fig 4.

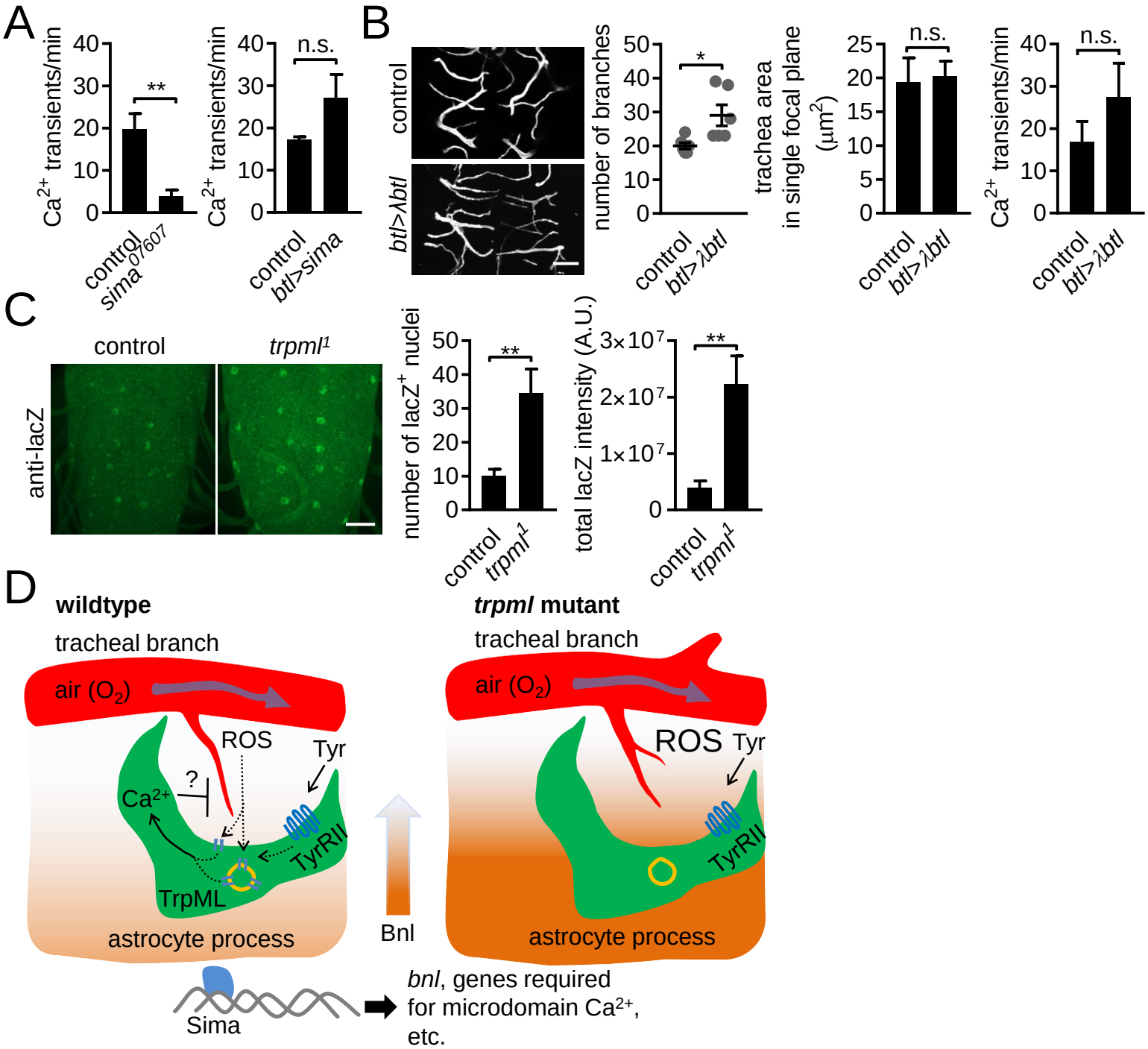
A
Ca2+ transients/min
40
30
20
10
0
**
control
sima0/607
n.s.
control
btl>sima
B
control
btl>λbtl
number of branches
*
trachea area in single focal plane (μm2)
25
20
15
10
5
C
control
trpml1
anti-lacZ
number of lacZ+ nuclei
total lacZ intensity (A.U.)
3×107
2×107
1×107
D
wildtype
tracheal branch
air (O2)
ROS
Tyr
?
Ca2+
TyrRII
TrpML
astrocyte process
Bnl
trpml mutant
Sima
bnl, genes required for microdomain Ca2+, etc.

Fig 5.

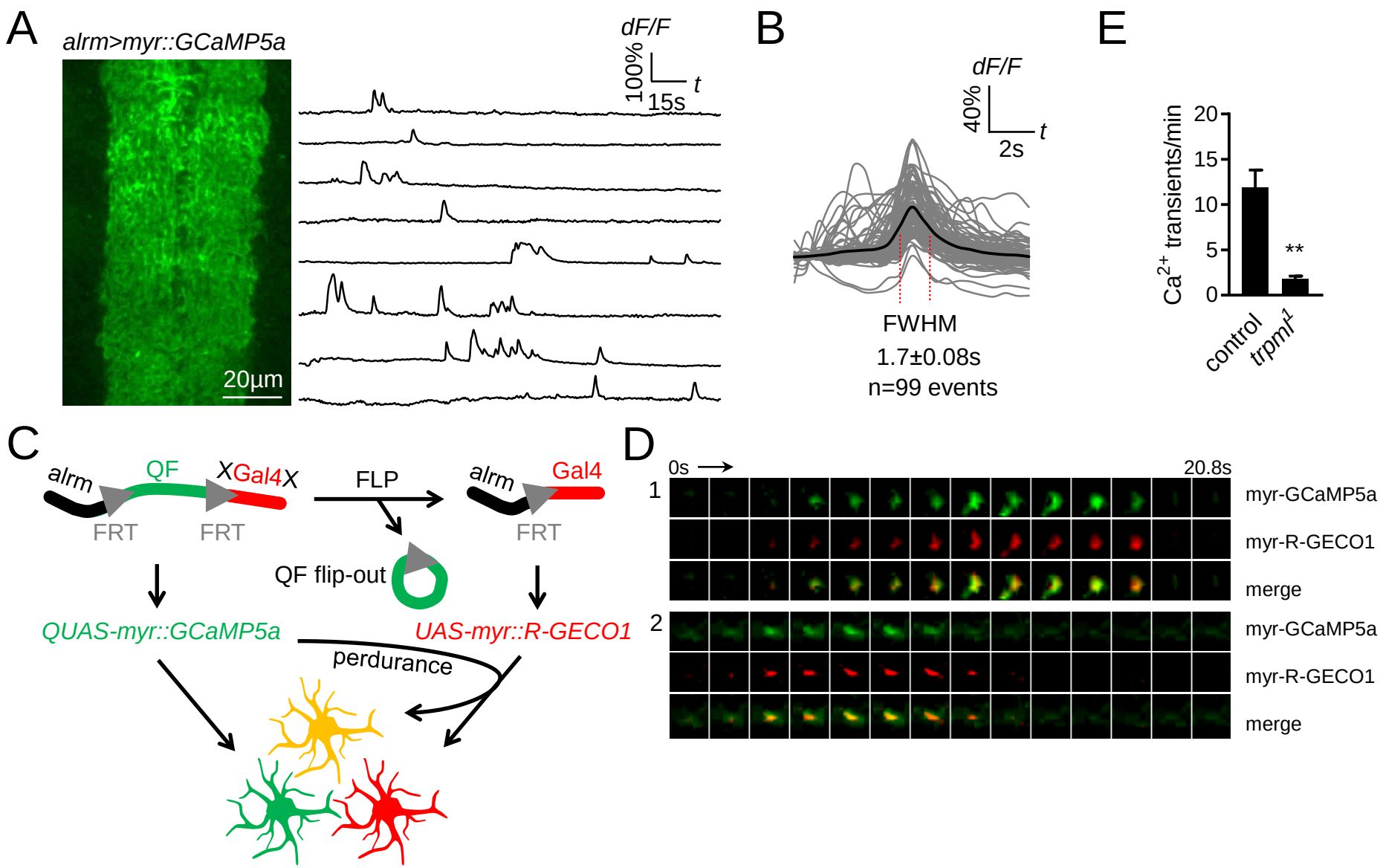
A
alrm>myr::GCaMP5a
20µm
dF/F
100%
t
15s
B
dF/F
40%
t
2s
FWHM
1.7±0.08s
n=99 events
E
Ca2+ transients/min
20
15
10
5
0
**
control
trpml1
C
alrm
QF
XGal4X
FRT
FRT
FLP
alrm
Gal4
FRT
QF flip-out
QUAS-myr::GCaMP5a
UAS-myr::R-GECO1
perdurance
D
0s
20.8s
1
2
myr-GCaMP5a
myr-R-GECO1
merge
myr-GCaMP5a
myr-R-GECO1
merge

Fig S1.

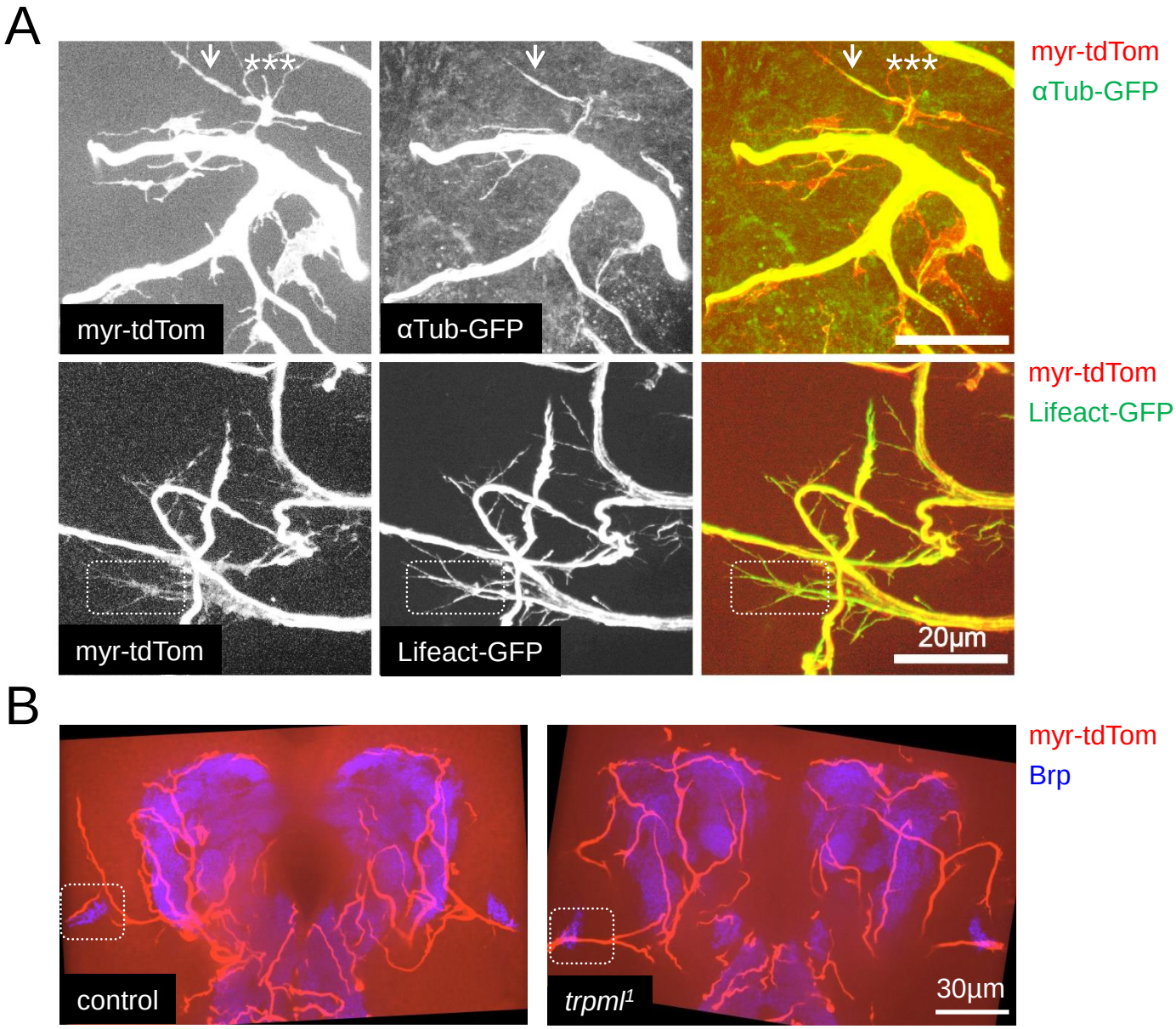
A
***
***
myr-tdTom
αTub-GFP
myr-tdTom
αTub-GFP
myr-tdTom
Lifeact-GFP
myr-tdTom
Lifeact-GFP
20μm
B
myr-tdTom
Brp
control
trpml1
30μm

Fig S2.

3rd instar

trachea autofluorescence

mpgTr traces

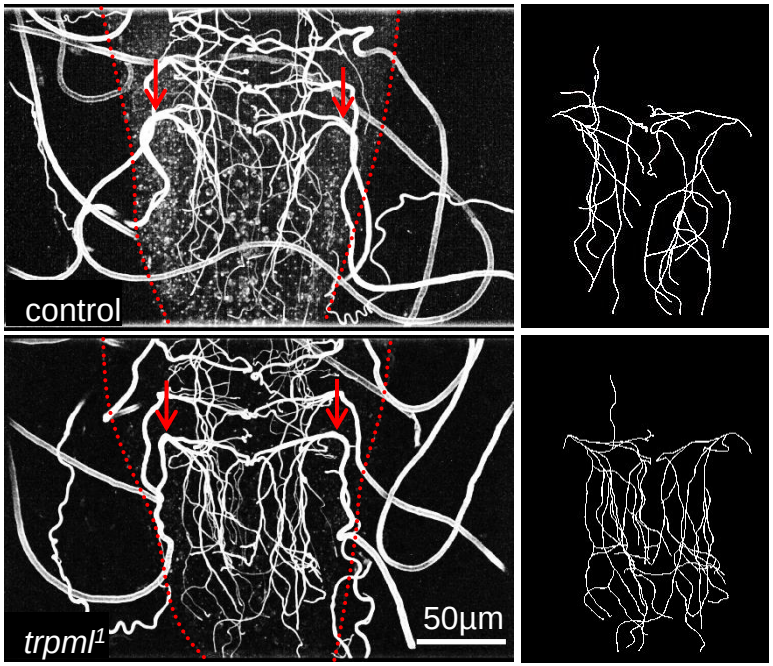

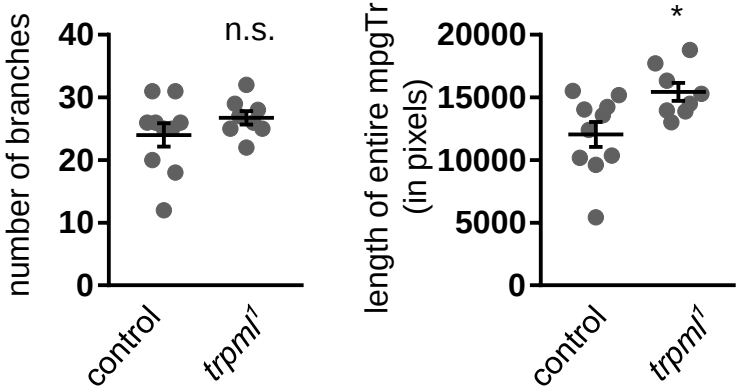

Fig S3.